

Theory of electron spin resonance in bulk topological insulators Bi_2Se_3 , Bi_2Te_3 and Sb_2Te_3

O Ly¹ and D M Basko²

¹ Institut de Physique et Chimie des Matériaux de Strasbourg, 67000 Strasbourg, France

² Laboratoire de Physique et Modélisation des Milieux Condensés, Université Grenoble Alpes and CNRS, B.P. 166, 38042 Grenoble, France

E-mail: ousmane.ly@ipcms.cnrs.fr

Abstract. We report a theoretical study of electron spin resonance in bulk topological insulators, such as Bi_2Se_3 , Bi_2Te_3 and Sb_2Te_3 . Using the effective four-band model, we find the electron energy spectrum in a static magnetic field and determine the response to electric and magnetic dipole perturbations, represented by oscillating electric and magnetic fields perpendicular to the static field. We determine the associated selection rules and calculate the absorption spectra. This enables us to separate the effective orbital and spin degrees of freedom and to determine the effective g factors for electrons and holes.

Submitted to: *J. Phys.: Condens. Matter*

1. Introduction

The discovery of Bi_2Se_3 , Bi_2Te_3 and Sb_2Te_3 being topological insulators [1, 2, 3, 4] has greatly stimulated research on these materials, the main object of interest being the existence of topologically protected conducting surface states [5]. The interest in bulk properties of these materials is driven by their high performance as thermoelectrics [6, 7, 8]. A powerful tool to probe electronic properties of solids is magneto-optical spectroscopy which was recently applied to bulk Bi_2Se_3 , where optical transitions between electronic Landau levels were observed [9].

The standard textbook picture of non-relativistic electron motion in a static uniform magnetic field involves Landau quantization of the orbital motion in the plane perpendicular to the field, and Zeeman splitting of the Landau levels according to the spin projection. The strength of the Zeeman splitting is characterized by the effective g factor. The orbital and spin degrees of freedom can be addressed separately by applying oscillating electric or magnetic field perpendicular to the static field, resulting respectively in transitions between orbital Landau levels (cyclotron resonance) or Zeeman sublevels (electron spin resonance, ESR, also called electron paramagnetic resonance). The ESR spectroscopy [10, 11] is a powerful tool for studying impurity electron spins, as well as those of conduction electrons [12, 13, 14, 15, 16, 17]. An ESR experiment in Bi_2Se_3 has recently been reported [18].

The simple picture of separation between orbital and spin degrees of freedom breaks down if a strong spin-orbit coupling is present. Indeed, solution of the effective

Schrödinger equation in the static magnetic field B_z gives a set of B_z -dependent energy levels [19], and it is not obvious how to separate the quantum numbers into effective orbital and spin ones, and how to define the effective g factors. At the same time, the response to physical perturbations, such as oscillating electric and magnetic fields, corresponding to the cyclotron resonance and ESR experiments, can be determined unambiguously. Then, one can try to analyze the corresponding transitions, with the aim of determining the effective orbital and spin degrees of freedom, and extracting the effective g factors. This is the subject of the present work.

2. The model

We use the effective model for 3D topological insulators Bi_2Se_3 , Bi_2Te_3 and Sb_2Te_3 proposed in [1]. The full microscopic derivation of this model is given in [19]. Neglecting terms of degree k^3 and higher, we start from the following Hamiltonian in the absence of the magnetic field:

$$H_{\mathbf{k}} = \varepsilon(\mathbf{k}) + \begin{pmatrix} \mathcal{M}(\mathbf{k}) & \mathcal{B}_0 k_z & 0 & \mathcal{A}_0 k_- \\ \mathcal{B}_0 k_z & -\mathcal{M}(\mathbf{k}) & \mathcal{A}_0 k_- & 0 \\ 0 & \mathcal{A}_0 k_+ & \mathcal{M}(\mathbf{k}) & -\mathcal{B}_0 k_z \\ \mathcal{A}_0 k_+ & 0 & -\mathcal{B}_0 k_z & -\mathcal{M}(\mathbf{k}) \end{pmatrix}, \quad (1)$$

leading to the energy spectrum :

$$E_{\mathbf{k}} = \varepsilon(\mathbf{k}) \pm \sqrt{\mathcal{M}(\mathbf{k})^2 + \mathcal{A}_0^2(k_x^2 + k_y^2) + \mathcal{B}_0^2 k_z^2}, \quad (2)$$

where $\varepsilon(\mathbf{k}) = C_1 k_z^2 + C_2(k_x^2 + k_y^2)$ (we omit the constant term C_0), $\mathcal{M}(\mathbf{k}) = M_0 + M_1 k_z^2 + M_2(k_x^2 + k_y^2)$, and we denoted $k_{\pm} = k_x \pm ik_y$. The band structure parameters $C_{1,2}, M_{0,1,2}, \mathcal{A}_0, \mathcal{B}_0$ have been estimated in [19] from a combination of *ab initio* calculations and $\mathbf{k} \cdot \mathbf{p}$ perturbation theory. Somewhat different values of parameters $C_2, M_0, M_2, \mathcal{A}_0$ have been proposed in [9] to match magneto-optical spectroscopy data for Bi_2Se_3 . Hamiltonian (1) is invariant under the time reversal:

$$U_{\text{T}} H_{-\mathbf{k}}^* U_{\text{T}}^{-1} = H_{\mathbf{k}}, \quad U_{\text{T}} = \begin{pmatrix} 0 & 0 & 1 & 0 \\ 0 & 0 & 0 & 1 \\ -1 & 0 & 0 & 0 \\ 0 & -1 & 0 & 0 \end{pmatrix}. \quad (3)$$

The Hamiltonian in the presence of an external magnetic field is obtained by the Peierls substitution $\mathbf{k} \rightarrow \boldsymbol{\pi} = -i\nabla + (e/\hbar c)\mathbf{A}$ in (1), where we assume the electron charge to be $-e$, and by including the gauge-invariant Zeeman-type terms [19]:

$$H_{\text{Z}} = \frac{\mu_{\text{B}}}{2} \begin{pmatrix} g_{1z} B_z & 0 & g_{1p} B_- & 0 \\ 0 & g_{2z} B_z & 0 & g_{2p} B_- \\ g_{1p} B_+ & 0 & -g_{1z} B_z & 0 \\ 0 & g_{2p} B_+ & 0 & -g_{2z} B_z \end{pmatrix}, \quad (4)$$

where μ_{B} is the Bohr magneton, $B_{\pm} = B_x \pm iB_y$, and the g -factors $g_{1z}, g_{2z}, g_{1p}, g_{2p}$ have been estimated in [19]. For a constant homogeneous field B_z along the z direction, we use the Landau gauge $A_x = -B_z y$, $A_y = A_z = 0$.

The electric dipole perturbation is obtained by applying a uniform oscillating electric field in the direction perpendicular to the constant magnetic field. As the system is isotropic in the xy plane, we can choose the x direction without the loss of generality. This corresponds to the following total vector potential:

$$A_x = -B_z y + \frac{c\mathcal{E}_x}{i\omega} e^{-i\omega t} + \text{c.c.}, \quad A_y = A_z = 0, \quad (5)$$

where \mathcal{E}_x is the electric field amplitude, and “c.c.” stands for complex conjugate. The magnetic dipole perturbation (without electric quadrupole contribution) corresponds to the vector potential [20]

$$A_x = -B_z y, \quad A_y = -\frac{B_x z}{2} e^{-i\omega t} + \text{c.c.}, \quad A_z = \frac{B_x y}{2} e^{-i\omega t} + \text{c.c.}, \quad (6)$$

which gives a uniform oscillating magnetic field along x , as well as a position-dependent oscillating electric field, $-(1/c)\partial\mathbf{A}/\partial t$. Indeed, by Faraday’s law, a time-dependent magnetic field is necessarily accompanied by an electric field.

In the following, we will calculate the energy absorbed by the system due to each of the two perturbations. We will use the general expression of the linear response theory for an electronic system whose single-particle Hamiltonian H contains a stationary part H_0 and a monochromatic perturbation,

$$H(t) = H_0 + F e^{-i\omega t} + F^\dagger e^{i\omega t}. \quad (7)$$

The power, absorbed by the system, is given by the sum over single-electron transitions $\beta \rightarrow \alpha$ whose rates are obtained from the Fermi Golden Rule [21]:

$$P(\omega) = 2\pi\omega \sum_{\alpha,\beta} |F_{\alpha\beta}|^2 (f_\beta - f_\alpha) \delta(E_\alpha - E_\beta - \hbar\omega), \quad (8)$$

where α, β label the eigenstates of H_0 with energies E_α, E_β and occupations f_α, f_β , and $F_{\alpha\beta}$ is the matrix element of the perturbation between these states.

3. Results

3.1. Landau levels

Landau levels for the described model were found in [19]. It is convenient to define the raising and lowering operators $\hat{a}^\dagger = \pi_+ l_B / \sqrt{2}$, $\hat{a} = \pi_- l_B / \sqrt{2}$, where $l_B = \sqrt{\hbar c / (e B_z)}$ is the magnetic length. The wave functions can be sought in the form

$$\psi(x, y, z) = \frac{e^{ik_x x + ik_z z}}{\sqrt{L_x L_z}} \begin{pmatrix} b_{n1} \phi_{n-1} \\ b_{n2} \phi_{n-1} \\ b_{n3} \phi_n \\ b_{n4} \phi_n \end{pmatrix}, \quad (9)$$

where $L_{x,y,z}$ is the size of the sample in the corresponding direction, $n \geq 0$ is the Landau level index, $\phi_n = \phi_n(k_x l_B^2 - y)$ are the normalized harmonic oscillator wave functions, and b_{nj} , $j = 1, \dots, 4$ are some unknown coefficients (b_{01} and b_{02} must vanish as ϕ_{-1} is not defined). In this representation, $\hat{a}\phi_n = \sqrt{n}\phi_{n-1}$, so the coefficients b_{nj} satisfy the 4×4 eigenvalue problem $(H_n - E)b_n = 0$ with the matrix H_n given by

$$H_n = \begin{pmatrix} \varepsilon_n + \mathcal{M}_n & \mathcal{B}_0 k_z & 0 & \sqrt{2n} \mathcal{A}_0 / l_B \\ \mathcal{B}_0 k_z & \varepsilon_n - \mathcal{M}_n & \sqrt{2n} \mathcal{A}_0 / l_B & 0 \\ 0 & \sqrt{2n} \mathcal{A}_0 / l_B & \varepsilon_n + \mathcal{M}_n & -\mathcal{B}_0 k_z \\ \sqrt{2n} \mathcal{A}_0 / l_B & 0 & -\mathcal{B}_0 k_z & \varepsilon_n - \mathcal{M}_n \end{pmatrix} + \frac{\mu_B B_z}{2} \begin{pmatrix} \tilde{g}_{1z} & 0 & 0 & 0 \\ 0 & \tilde{g}_{2z} & 0 & 0 \\ 0 & 0 & -\tilde{g}_{1z} & 0 \\ 0 & 0 & 0 & -\tilde{g}_{2z} \end{pmatrix}, \quad (10)$$

where we denoted $\varepsilon_n = 2nC_2/l_B^2 + C_1 k_z^2$, $\mathcal{M}_n = M_0 + 2nM_2/l_B^2 + M_1 k_z^2$, $\tilde{g}_{1z} = g_{1z} - 4m_0(C_2 + M_2)/\hbar^2$, $\tilde{g}_{2z} = g_{2z} - 4m_0(C_2 - M_2)/\hbar^2$, and m_0 stands for the free electron mass entering the Bohr magneton $\mu_B = e\hbar/(2m_0c)$.

The matrix H_n from (10) cannot be diagonalized analytically, however, some general properties of the spectrum can be established:

- (i) the energy does not depend on k_x , which determines the usual degeneracy $L_x L_y / (2\pi l_B^2)$ of each Landau level;
- (ii) for each k_z , there are four energy levels, $E_{nj}(k_z)$, $j = 1, \dots, 4$, for $n > 0$, while for $n = 0$ there are only two levels;
- (iii) at $k_z = 0$, the Hamiltonian splits in two decoupled 2×2 blocks.

To determine the dispersion for $k_z \neq 0$, one can use perturbation theory in $v_z = (1/\hbar)(\partial H_{\mathbf{k}}/\partial k_z)$, which has no diagonal matrix elements within the blocks at $k_z = 0$. Thus, the dispersion has no linear term in k_z , so one can approximate it by a quadratic one near $k_z = 0$: $E_{nj}(k_z) \approx E_{nj}(0) + \alpha_{nj} k_z^2$. As a result, the joint density of states has a series of square-root-type singularities near frequencies corresponding to transition energies $E_{n'j'}(0) - E_{nj}(0)$ at $k_z = 0$:

$$\begin{aligned} P(\omega) &= 2\pi\hbar\omega \sum_{n,j,n',j'} \frac{L_x L_y}{2\pi l_B^2} \int \frac{L_z dk_z}{2\pi} |F_{nj,n'j'}(k_z)|^2 \times \\ &\quad \times \delta(E_{n'j'}(k_z) - E_{nj}(k_z) - \hbar\omega) \approx \\ &\approx \sum_{n,j,n',j'} \frac{\omega |F_{nj,n'j'}(0)|^2 L_x L_y L_z / (2\pi l_B^2)}{\sqrt{|\alpha_{n'j'} - \alpha_{nj}|(\hbar\omega + E_{nj}(0) - E_{n'j'}(0))}}, \end{aligned} \quad (11)$$

where we took into account the fact that k_z is not changed under the excitation, and the summation is over levels n, j which are filled, and n', j' which are empty. In a real sample, these singularities are smeared due to level broadening (e. g., by disorder), so experimental spectra consist of broadened peaks located near transition energies $E_{n'j'}(0) - E_{nj}(0)$ (asymmetric peak smearing may also lead to a shift of the maximum frequency). Their intensities are determined by the perturbation matrix elements between states at $k_z = 0$.[‡]

At $k_z = 0$, Hamiltonian (10) consists of two independent 2×2 blocks. We label the outer/inner block by $\sigma = \uparrow, \downarrow = \pm 1$, respectively. Besides n and σ , the levels with $n > 0$ are also labeled by the band index $\lambda = \pm 1$. Their energies are given by

$$\begin{aligned} E_{n>0,\sigma,\lambda} &= \lambda \sqrt{\frac{2n}{l_B^2} \mathcal{A}_0^2 + \left[M_0 + \frac{2nM_2}{l_B^2} - \frac{\sigma}{l_B^2} \left(C_2 - \frac{g_{1z} + g_{2z}}{8m_0/\hbar^2} \right) \right]^2} \\ &\quad + \frac{2nC_2}{l_B^2} - \frac{\sigma}{l_B^2} \left(M_2 - \frac{g_{1z} - g_{2z}}{8m_0/\hbar^2} \right), \end{aligned} \quad (12)$$

$$E_{n=0,\sigma=\pm 1} = \frac{C_2}{l_B^2} \mp \left(M_0 + \frac{M_2}{l_B^2} \right) - g_{2z,1z} \frac{\mu_B B_z}{2}. \quad (13)$$

Corrections to the Landau level energies, $\alpha_{n\sigma\lambda} k_z^2$, can then be obtained by perturbation theory for Hamiltonian (10) in $C_1 k_z^2$, $M_1 k_z^2$ (to the first order), and in $\mathcal{B}_0 k_z$ (to the second order).

We emphasize that at this point, σ is just a quantum number introduced formally in order to distinguish between the two blocks at $k_z = 0$. Its relation to the spin degree of freedom will be established below by studying the response to physical perturbations. Note, however, that the two sectors are exchanged by the time reversal operation (3), as is also the case for the real spin.

[‡] One should be cautious when applying this argument to intraband transitions at low fields. Indeed, at $B_z \rightarrow 0$, all $\alpha_{n,j} \rightarrow C_1 \pm [M_1 + \mathcal{B}_0^2/(2M_0)]$, so the denominator in (11) vanishes. The peak shape is then determined mostly by the broadening and by higher-order in k_z terms in $E_{nj}(k_z)$.

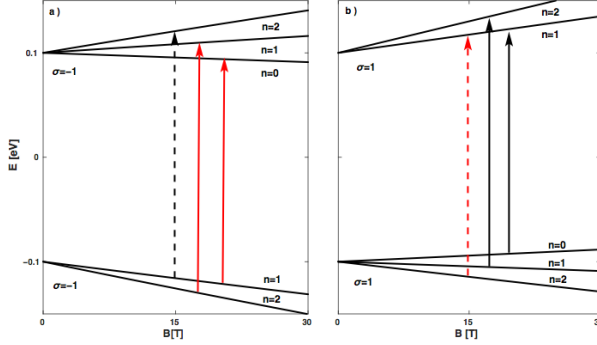


Figure 1. Interband transverse electric dipole transitions for the first three Landau levels for $\sigma = \pm 1$ [panels (a) and (b), respectively]. Solid and dashed arrows show dominant and subdominant transitions. Left and right circular polarizations are shown by black and red arrows, respectively.

3.2. Electric dipole perturbation

The perturbation, corresponding to the vector potential (5), is given by

$$F_e = \frac{ie\mathcal{E}_x}{\omega} v_x, \quad \mathbf{v} \equiv \frac{1}{\hbar} \frac{\partial H_{\mathbf{k}}}{\partial \mathbf{k}} \Big|_{\mathbf{k} \rightarrow \boldsymbol{\pi}}, \quad (14)$$

and the absorbed power found from (8) is related to the real part of the optical conductivity $\sigma_{ij}(\omega)$ as

$$P(\omega) = 2 \text{Re} \sigma_{xx}(\omega) |\mathcal{E}_x|^2 L_x L_y L_z. \quad (15)$$

At $k_z = 0$, the evaluation of the matrix elements of F_e is straightforward, but the resulting expressions are cumbersome, so we do not give them here. F_e has no matrix elements between different σ sectors, so the selection rules are

$$n, \sigma, \lambda \rightarrow n \pm 1, \sigma, \lambda', \quad (16)$$

with no restriction on λ, λ' (note, however, that for interband transitions, some matrix elements can be much stronger than others, as discussed in the end of section 4). Representing the linear polarization as a sum of two circular polarizations, one can see that the plus/minus sign corresponds to the counterclockwise/clockwise rotating electric field (left/right circular polarization), respectively.

In Figures 1, 2, we show allowed transitions for a few Landau levels, as well as the corresponding absorption spectra, calculated using (8) with the energies and matrix elements obtained by numerically diagonalizing (10) for each k_z , without employing the parabolic approximation for $E_{nj}(k_z)$. We use the parameters given in [9] for Bi_2Se_3 : $C_2 = 3 \text{ eV} \cdot \text{\AA}^2$, $M_0 = 0.1 \text{ eV}$, $M_2 = -22.5 \text{ eV} \cdot \text{\AA}^2$, $\mathcal{A}_0 = 3.1 \text{ eV} \cdot \text{\AA}$, $g_{1z} = g_{2z} = 0$, which determine the peak positions. The peak widths are determined by the k_z dependence of the energies, and we take the corresponding parameters from [19]: $C_1 = 5.7 \text{ eV} \cdot \text{\AA}^2$, $M_1 = -6.9 \text{ eV} \cdot \text{\AA}^2$, $\mathcal{B}_0 = 2.3 \text{ eV} \cdot \text{\AA}$. To cut off the square-root singularities, we replace the δ function in (8) by a Lorentzian with full width at half maximum 2γ , setting $\gamma = 0.5 \text{ meV}$.

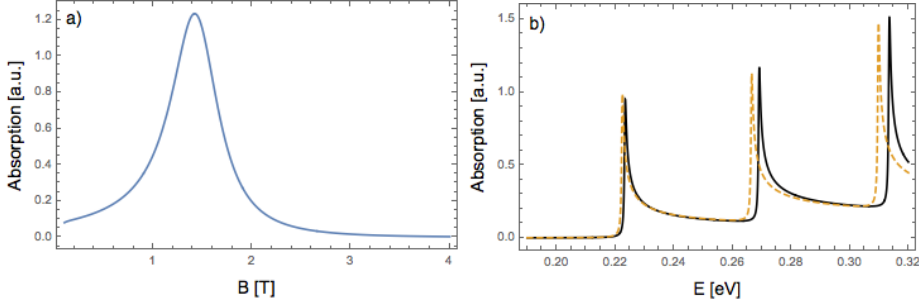


Figure 2. (a) Cyclotron resonance spectrum of bulk n -doped Bi_2Se_3 as a function of the magnetic field at fixed microwave frequency $f = \omega/(2\pi) = 300\text{GHz}$. The electron concentration $n_e = 10^{17}\text{cm}^{-3}$, the temperature is taken 5 K. (b) Optical absorption spectrum of bulk undoped Bi_2Se_3 as a function of the photon energy $E = \hbar\omega$ at fixed $B_z = 30\text{ T}$. The solid and dashed curves correspond to the left and right circular polarizations. The band structure parameters are taken from [9] and [19] (see main text for details).

3.3. Magnetic dipole perturbation

The corresponding perturbation contains three terms:

$$F_m = -\frac{eB_x}{2c} z v_y + \frac{eB_x}{2c} y v_z + \frac{\mu_B B_x}{2} \begin{pmatrix} 0 & 0 & g_{1p} & 0 \\ 0 & 0 & 0 & g_{2p} \\ g_{1p} & 0 & 0 & 0 \\ 0 & g_{2p} & 0 & 0 \end{pmatrix}. \quad (17)$$

The matrix elements of the first term (which we denote by F_{m1}) are found using the separability of wave functions (9). For the transverse motion, the treatment of v_y is totally analogous to that of v_x for the electric dipole case, while the matrix element of z is more conveniently evaluated if one imposes hard wall boundary conditions at $z = \pm L_z/2$ and uses the standing waves $\sin k_z z$, $\cos k_z z$ instead of the propagating ones $e^{ik_z z}$. After some algebra [22], the resulting contribution of F_{m1} to the absorption can be represented as

$$P_{e\perp}(\omega) = 2 \text{Re } \sigma_{yy}(\omega) L_x L_y \int_{-L_z/2}^{L_z/2} |\mathcal{E}_y(z)|^2 dz, \quad (18)$$

where the transverse electric field $\mathcal{E}_y(z) = -(\omega z/2c)B_x$ is the one given by the Faraday's law. The selection rules are the same as for the electric dipole case, (16).

In the second term of (17), v_z contains (i) terms originating from $\partial\mathcal{E}/\partial k_z$, $\partial\mathcal{M}/\partial k_z$, and (ii) a term $\propto \mathcal{B}_0$. The former ones are proportional to k_z , so we neglect them as we are interested in transitions at $k_z = 0$. The term (ii) can be combined with the third term in (17), to give

$$F_{m2} = \frac{eB_x}{2m_0\hbar c} \begin{pmatrix} 0 & m_0\mathcal{B}_0 y & g_{1p}\hbar^2/2 & 0 \\ m_0\mathcal{B}_0 y & 0 & 0 & g_{2p}\hbar^2/2 \\ g_{1p}\hbar^2/2 & 0 & 0 & -m_0\mathcal{B}_0 y \\ 0 & g_{2p}\hbar^2/2 & -m_0\mathcal{B}_0 y & 0 \end{pmatrix}. \quad (19)$$

F_{m2} induces transitions between sectors with different σ , so it does not interfere with the σ -conserving F_{m1} . When calculating the matrix elements of F_{m2} , we encounter

$$\langle\phi_n|y|\phi_{n'}\rangle = k_x l_B^2 \delta_{nn'} - l_B \sqrt{\frac{n'}{2}} \delta_{n',n+1} - l_B \sqrt{\frac{n}{2}} \delta_{n,n'+1}. \quad (20)$$

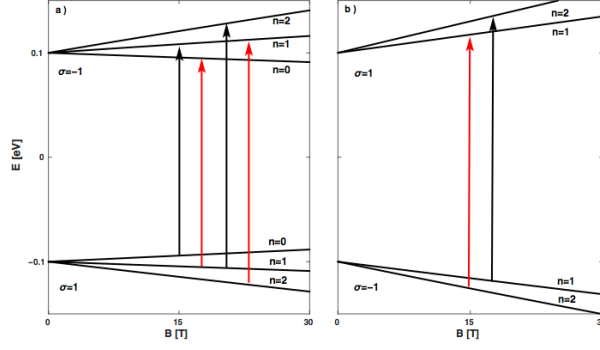


Figure 3. Same as in Figure 1, but magnetic dipole transitions are shown.

The term $k_x l_B^2 \delta_{nn'}$ gives rise to absorption which can be identified as

$$P_{ez}(\omega) = 2 \operatorname{Re} \sigma_{zz}(\omega) L_x L_z \int_{-L_y/2}^{L_y/2} |\mathcal{E}_z(y)|^2 dy, \quad (21)$$

with $\mathcal{E}_z(y) = (\omega y/2c)B_x$ from the Faraday's law (indeed, $k_x l_B^2$ is the y coordinate of the cyclotron orbit guiding center). The intraband matrix elements of the $\delta_{nn'}$ term vanish at $k_z = 0$ because of the matrix structure; this term produces a finite intraband absorption only when combined with the first order in k_z , which flips the spin back. The resulting intraband absorption is represented by the Drude peak at $\omega = 0$ (as the electron motion in the z direction remains free), which is beyond the scope of our analysis. In the interband absorption spectrum, the $\delta_{nn'}$ term does produce additional peaks.

Only the last two terms in (20) produce new transitions which are not contained in $\sigma_{ij}(\omega)$, and thus can be associated with magnetic dipole. The corresponding selection rules are

$$n, \sigma, \lambda \rightarrow n \pm 1, -\sigma, \lambda'. \quad (22)$$

We show these magnetic transitions for a few Landau levels in figure 3 as well as the absorption spectrum in figure 4. The spectrum contains (i) the same peaks as in figure 2, due to contribution (18) from the transverse electric dipole, (ii) peaks due to the z component of the electric dipole, contribution (21), whose frequencies turn out to be very close to those of the previous series, and (iii) magnetic peaks, seen as very weak features near the energies 0.20, 0.25, 0.29 eV. The relative intensity of the weak third series with respect to the two first ones depends on the sample size. Indeed, for a given strength of the transverse magnetic field B_x , the typical values of the electric field components in the sample are $\mathcal{E}_y \sim (\omega L_z/c)B_x$, $\mathcal{E}_z \sim (\omega L_y/c)B_x$ [as (6) assumes the sample to be placed in the node of the electric field]. Thus, quite a small value $L_{x,y,z} = 100$ nm was chosen to calculate the interband spectra in Figure 4, in order for the magnetic peaks to be noticeable. Some estimates for the relative intensities are given in the next section.

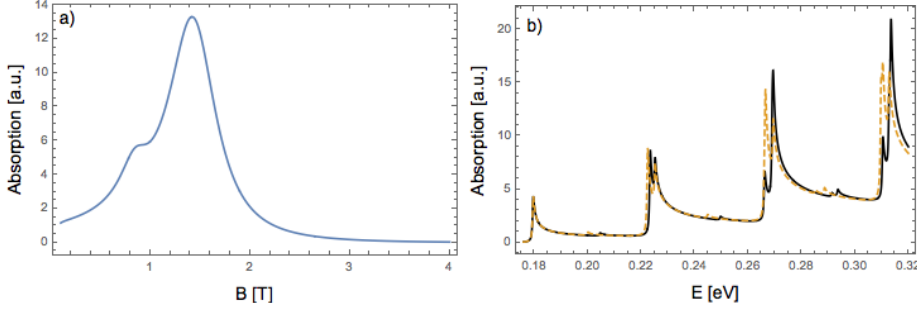


Figure 4. (a) Intraband absorption (ESR) spectrum of an n -doped Bi_2Se_3 sample of thickness $L_z = 500$ nm. (b) Interband absorption spectrum of a Bi_2Se_3 sample with size $L_{x,y,z} = 100$ nm subject to a constant magnetic field $B_z = 30$ T and an oscillating transverse magnetic field. All other parameters and notations are the same as for Figure 2.

4. Transitions' classification and the g factors

For the subsequent discussion we have to specify the sign of the gap parameter M_0 . In fact, this sign is just a matter of convention. Indeed, if in the Hamiltonian (1), (4) one changes simultaneously the signs of $M_{0,1,2}$ and exchanges the inner and outer blocks (the two sectors with different σ) which also implies the exchange $g_{1z} \leftrightarrow g_{2z}$, $g_{1p} \leftrightarrow g_{2p}$, the Hamiltonian remains intact. We prefer the $M_0 > 0$ convention, as then Hamiltonian (1) has the same structure as the Dirac Hamiltonian in quantum electrodynamics [23]. In fact, the Dirac Hamiltonian is given by (1) with $\varepsilon(\mathbf{k}) = 0$, $\mathcal{M}(\mathbf{k}) = m_0 \hbar^2 c^2$, $\mathcal{A}_0 = \mathcal{B}_0 = \hbar c$. In the following, we will identify different transitions using the analogy with the non-relativistic limit of the Dirac Hamiltonian, which corresponds to the low-energy or low- B_z limit $|E_{n,\sigma,\lambda}| - M_0 \ll M_0$.

If $M_0 > 0$, then $n = 0$, $\sigma = -1$ (\downarrow) level is associated with the conduction band ($\lambda = +1$), and $n = 0$, $\sigma = +1$ (\uparrow) with the valence band ($\lambda = -1$). To match the non-relativistic limit, we shift the n index down by 1 for half of the levels: $\tilde{n} = n - \lambda\sigma/2 - 1/2$, so that for each $\tilde{n} \geq 0$ we have four levels with $\sigma = \pm 1$, $\lambda = \pm 1$.

First, consider intraband transitions. The electric dipole selection rule (16) remains the same in the new representation: $\tilde{n}, \sigma \rightarrow \tilde{n} \pm 1, \sigma$. These transitions are associated with the cyclotron resonance. The magnetic dipole selection rules (22) in the new representation are listed in Table 1. Since a left/right circularly polarized photon carries an angular momentum of ± 1 , we can associate \tilde{n} and $\sigma/2$ with the effective orbital and spin angular momentum for electrons in the conduction band. For holes in the valence band, these would be $-\tilde{n}$ and $\sigma/2$, respectively. The transitions $\tilde{n}, \sigma \rightarrow \tilde{n}, -\sigma$ can be identified with the electron spin resonance. For the Dirac Hamiltonian, these transitions correspond to the electron spin flip in the non-relativistic limit, while the transitions with \tilde{n} changing by ± 2 are due to spin-orbit coupling, and thus are weak. Thus, it is natural to define the effective g -factors for electrons in the conduction band and for the holes in the valence band as

$$g_e = \frac{1}{\mu_B} \left. \frac{\partial(E_{n,\downarrow,+1} - E_{n+1,\uparrow,+1})}{\partial B_z} \right|_{B_z=0} = -\frac{2m_0 \mathcal{A}_0^2}{M_0} - g_{1z}, \quad (23a)$$

$$g_h = \frac{1}{\mu_B} \left. \frac{\partial(-E_{n+1,\downarrow,-1} + E_{n,\uparrow,-1})}{\partial B_z} \right|_{B_z=0} = \frac{2m_0 \mathcal{A}_0^2}{M_0} - g_{2z}. \quad (23b)$$

	\odot	\ominus
conduction band	$\tilde{n}, \downarrow \rightarrow \tilde{n}, \uparrow$ $\tilde{n}, \uparrow \rightarrow \tilde{n}+2, \downarrow$	$\tilde{n}, \uparrow \rightarrow \tilde{n}, \downarrow$ $\tilde{n}, \downarrow \rightarrow \tilde{n}-2, \uparrow$
valence band	$\tilde{n}, \uparrow \rightarrow \tilde{n}, \downarrow$ $\tilde{n}, \downarrow \rightarrow \tilde{n}+2, \uparrow$	$\tilde{n}, \downarrow \rightarrow \tilde{n}, \uparrow$ $\tilde{n}, \uparrow \rightarrow \tilde{n}-2, \downarrow$

Table 1. Magnetic dipole selection rules for intraband transitions. The left and right circular polarizations are labeled by \odot and \ominus , respectively.

Note that $g_e < 0$ because the electron charge is negative and $\mu_B > 0$, while $g_h > 0$ as the hole has a positive charge. The numerical values from [9] give $g_h = -g_e \approx 26$.

As intraband transitions are usually probed at low magnetic fields, the relative strengths of different transitions can be reliably estimated in the “non-relativistic limit” using the expansion in small parameters $\sqrt{n}\mathcal{A}_0/(l_B M_0) \ll 1$, $nM_2/(l_B^2 M_0) \ll 1$. By evaluating the ratio of the squares of the corresponding matrix elements at $k_z = 0$, we find that the ESR transitions are weaker than the cyclotron resonance by a factor $\sim (1/8n)(B_x/\mathcal{E}_x)^2(\mathcal{B}_0/\mathcal{A}_0)^2(\omega l_B/c)^2$. The transitions with $\Delta\tilde{n} = \pm 2$ are weaker than the ESR ones by an additional factor

$$\eta \sim \left(n \frac{\mathcal{A}_0^2 + 4M_0 M_2}{2M_0^2 l_B^2} \right)^2 \quad (24)$$

(note the strong cancellation between the two terms in the numerator for the parameters of Bi_2Se_3 [9]).

For transitions from the valence to the conduction band, the dominant transverse electric dipole transitions in the non-relativistic limit are those with $\tilde{n} \rightarrow \tilde{n}$, occurring in $\sigma = +1$ and $\sigma = -1$ sectors for the left and right circular polarizations, respectively. They are accompanied by transitions with $\Delta\tilde{n} = \pm 2$, whose intensity is weaker at low fields by the same factor η as in (24) [note though that the relevant magnetic fields are much higher than for the intraband transitions, and they are out of the “non-relativistic” limit, so (24) provides only an order-of-magnitude estimate]. Among the magnetic dipole interband transitions, $\tilde{n}, \sigma \rightarrow \tilde{n} \pm 1, -\sigma$, there is no dominant series, they all have similar strength. The ratio between the strength of the interband magnetic dipole transitions and the leading series of the transverse electric dipole transitions can be estimated as $\sim (n/8)(B_x/\mathcal{E}_x)^2(\mathcal{B}_0/\mathcal{A}_0)^2(\omega l_B/c)^2$, also similar to that in the intraband case. As both are proportional to $l_B^2 \propto 1/B_z$, the magnetic dipole peaks are more easily observed on top of the electric dipole ones for the intraband transitions than for the interband ones. Hence, a larger size is chosen for the former ones than for the latter to calculate the spectra shown in Figure 4. The ratio between the transverse and z electric dipole transitions is simply $(\mathcal{E}_x/\mathcal{E}_z)^2(\mathcal{A}_0/\mathcal{B}_0)^2$.

5. Conclusions

We have studied the bulk response of topological insulators Bi_2Se_3 , Bi_2Te_3 and Sb_2Te_3 in a static magnetic field to electric dipole and magnetic dipole perturbations. It corresponds to cyclotron resonance, electron spin resonance and interband optical absorption. Using the effective four-band model [1, 19], we found the Landau levels in the static magnetic field, and calculated the energy absorption spectrum when an oscillating electric or magnetic field is applied perpendicular to the static magnetic

field. We have determined the corresponding selection rules; for intraband transitions they are the same as for genuine Dirac electrons in quantum electrodynamics. From these selection rules, we were able to separate the effective orbital and spin degrees of freedom and deduce the effective g factors for electrons and holes.

Acknowledgments

The authors are grateful to M. Orlita and M. Potemski for very stimulating discussions and critical reading of the manuscript. O. Ly thanks Laboratoire de Physique et Modélisation des Milieux Condensés for hospitality and support during his undergraduate internship when this work started.

References

- [1] Zhang H, Liu C-X, Qi X-L, Dai X, Fang Z and Zhang S-C 2009 *Nature Phys.* **5** 438
- [2] Xia Y, Qian D, Hsieh D, Wray L, Pal A, Lin H, Bansil A, Grauer D, Hor Y S, Cava R J and Hasan M Z 2009 *Nature Phys.* **5** 398
- [3] Chen Y L, Analytis J G, Chu J-H, Liu Z K, Mo S K, Qi X L, Zhang H J, Lu D H, Dai X, Fang Z, Zhang S C, Fisher I R, Hussain Z and Shen Z-X 2009 *Science* **325** 178
- [4] Hsieh D, Xia Y, Qian D, Wray L, Dil J H, Meier F, Osterwalder J, Patthey L, Checkelsky J G, Ong N P, Fedorov A V, Lin H, Bansil A, Grauer D, Hor Y S, Cava R J and Hasan M Z 2009 *Nature* **460** 1101
- [5] Bernevig B A 2013 *Topological Insulators and Topological Superconductors* (Princeton University Press)
- [6] Hor Y S, Richardella A, Roushan P, Xia Y, Checkelsky J G, Yazdani A, Hasan M Z, Ong N P and Cava R J 2009 *Phys. Rev. B* **79** 195208
- [7] Kadel K, Kumari L, Li W Z, Huang J Y and Provencio P P 2011 *Nanoscale Res Lett* **6** 57
- [8] Osterhage H, Gooth J, Hamdou B, Gwozdz P, Zierold R and Nielsch K 2014 *Appl. Phys. Lett.* **105** 123117
- [9] Orlita M, Piot B A, Martinez G, Sampath Kumar N K, Faugeras C, Potemski M, Michel C, Hankiewicz E M, Brauner T, Schreyeck S, Brüne C, Buhmann H and Molenkamp L W 2015 *Phys. Rev. Lett.* **114** 186401
- [10] Zavoisky E K 1945 *J. Phys. USSR* **9** 221
- [11] Abragam A and Bleaney B 1970 *Electron Paramagnetic Resonance of Transition Ions* (Clarendon)
- [12] Griswold T W, Kip A F and Kittel C 1952 *Phys. Rev.* **88** 951
- [13] Dyson F J 1955 *Phys. Rev.* **98** 349
- [14] Lampe M and Platzman P M 1966 *Phys. Rev.* **150** 340
- [15] Seck M, Potemski M and Wyder P 1997 *Phys. Rev. B* **56** 7422.
- [16] Wilamowski Z, Jantsch W, Malissa H and Rössler U 2002 *Phys. Rev. B* **66** 195315
- [17] Rieger P 2007 *Electron Spin Resonance. Analysis and Interpretation*
- [18] Wolos A, Drabinska A, Szyszko S, Kaminska M, Strzelecka S G, Hruban A, Materna A and Piersa M 2013 AIP Conf. Proc. **1566** 197
- [19] Liu C-X, Qi X-L, Zhang H, Dai X, Fang Z and Zhang S-C 2010 *Phys. Rev. B* **82** 045122
- [20] Jackson J D 1975 *Classical Electrodynamics* (Wiley)
- [21] Landau L D and Lifchitz E M 1977 *Quantum mechanics* (Butterworth-Heinemann)
- [22] Ly O 2014 *Electron spin resonance in topological insulators: Theoretical study* (Master Thesis, University of Strasbourg).
- [23] Berestetskii V B, Lifshitz E M and Pitaevskii L P 1982 *Quantum Electrodynamics* (Butterworth-Heinemann)